2018 21st International Conference on Intelligent Transportation Systems (ITSC)
Maui, Hawaii, USA, November 4-7, 2018

Speed Planning for Autonomous Driving via Convex Optimization

Yu Zhang, Huiyan Chen, Steven L. Waslander, Tian Yang, Sheng Zhang, Guangming Xiong†, and Kai Liu

***Abstract*— In this paper, we present a convex-optimization-based method to solve speed planning problems over a fixed path for autonomous driving in both static and dynamic environments. Our contributions are twofold. First, we introduce a general, flexible and complete speed planning optimization which includes time efficiency, smoothness objectives and dynamics, friction circle, boundary condition constraints which addresses limitations of existing methods and is able to provide smooth, safety-guaranteed, dynamically-feasible, and time-efficient speed profiles. Second, we demonstrate that our problem preserves convexity with the expanded set of constraints, and hence, global optimality of solutions is guaranteed. We show how our formulation can be used in speed planning for various autonomous driving scenarios by providing several typical case studies in both static and dynamic environments. The results depict that the proposed method outperforms existing speed planners for autonomous driving in terms of capacity, optimality, safety and mobility.**

I. INTRODUCTION

Speed planning plays an important role in guaranteeing ride comfort and vehicle safety in autonomous driving applications. Speed planning methods used in the literature fall into two categories roughly: coupled speed planning and decoupled speed planning. The former category exists in motion planning frameworks that explore the spatial-temporal space simultaneously using optimization techniques [1] or search algorithms [2]. The latter category frequently appears in hierarchy motion planning frameworks [3], [4] that decouple motions by planning a path first and then constructing a speed profile along the path, or appears as a standalone research with the assumption that the path is known. As we focus on the second class of the problem, we review methods that are closely related to ours, which generates speed profiles along a fixed path subject to certain constraints.

Li *et al.* [4] employed a trapezoidal speed profile with constant accelerations along the fixed path and smoothed the ramp-up and ramp-down parts of trapezoidal speed profiles with 3^{rd}-order polynomials, which is neither optimal nor flexible. Further, the acceleration value may exceed the threshold after smoothing. Thus, very conservative accelerations for the ramp-up and decelerations for the ramp-down were selected in their work.

Gu *et al.* [3] developed a constraint-based speed planner that trimmed the reference speed profile according to speed limits, acceleration box constraints, and jerk thresholds iteratively. They considered moving obstacles in speed planning in a reactive way based on the distance between obstacles and the ego car to affect speed profiles. As dynamics constraints are considered separately in box form, their upper boundaries need to be selected conservatively to prevent the total force from exceeding the friction force limits, the capacity of driving at the limits to deal with emergencies or pursue time efficiency is somewhat restricted. The difference between the potential solution space of acceleration box constraints and friction circle constraints is shown in Fig. 1(a). In addition, reductions in the friction coefficient in extreme weather conditions will shrink the friction circle and the original fixed acceleration box constraints may create dangerous zones in the solution space, as shown in Fig. 1(a), which will inevitably lead to potential safety issues.

TABLE I: Constraints and Capacity of Different Methods

(a) Constraints
□: safety △: performance

Category	Constraint Name	Description	Property
Soft Constraints	Smoothness (S)	continuity of speeds over the path	△
	Time Efficiency (TE)	time used by travelling along the path	△
Hard Constraints	Friction Circle (FC)	total force should be within the friction circle	□
	Time Window (TW)	time window to reach a certain point on path	□ & △
	Boundary Condition (BC)	speed at the end of the path	□ & △

(b) Capacity of Different Methods

Method	S	TE	FC	TW	BC	Optimality	Safety	Mobility
Li *et al.* [4]	✓	✗	✗	✗	✓	✗	low	low
Gu *et al.* [3]	✓	✗	✗	✗	✓	✗	medium	medium
Dakibay *et al.* [5]	✗	✗	✓	✗	✓	✗	medium	high
Liu *et al.* [6]	✓	✓	✗	✓	✓	local	medium	medium
Lipp *et al.* [7]	✗	✓	✓	✗	✗	global	low	high
Ours	✓	✓	✓	✓	✓	global	high	high

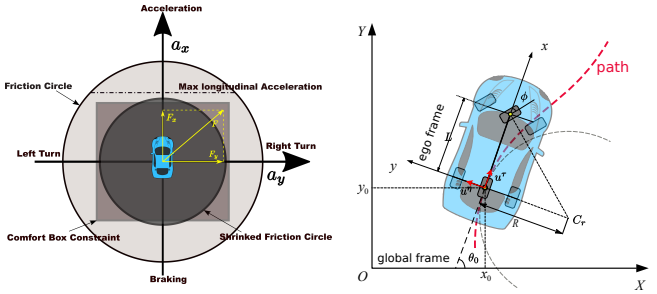

(a) Friction Circles (b) Single track car model

Fig. 1: Vehicle dynamics

Dakibay *et al.* [5] exploited an aggressive speed planning method by numerically solving a nonlinear differential equation (NDE) representation of the friction circle constraints. Due to the approximation of the solution of NDEs, the full capacity of the car's capabilities is not exploited. None of

Y. Zhang, H. Chen, G. Xiong, S. Zhang, T. Yang and K. Liu are with the School of Mechanical Engineering , Beijing Institute of Technology, Beijing, 10086 China (e-mail: yu.zhang.bit@gmail.com).

Steven L. Waslander is with the University of Toronto Institute of Aerospace Studies, Toronto, ON M3H 5T6, Canada (e-mail: stevenw@utias.utoronto.ca)

their acceleration points reaches the friction circle boundary exactly. As the driving conditions are quite close to the limits, admissible room left for track errors is little. We argue that the smoothness of speed profiles still needs to be considered to improve tracking performance of the controller for safety concerns (jerky speed profiles may result in overshooting and oscillation of controllers).

Lipp *et al*. [7] presented a convex-optimization-based general minimum time speed planning method over a fixed path. The friction circle constraint is well considered as a convex set constraint acting on the problem formulation, which leads to an elegant solution. However, smoothness of the speed profile is not considered, which most likely results in tracking performance and safety issues. Their method does not handle dynamic obstacles and includes no provision for stopping at the end of the path due to a lack of final state constraints.

Liu *et al*. [6] recently introduced a temporal optimization approach, optimizing time stamps for all waypoints along a fixed path with respect to time window constraints at each point, and then using a slack convex feasible set algorithm to solve the problem iteratively. However, the time efficiency is considered in an indirect way that minimizes speed deviations with respect to a reference speed over the path. Their formulation leads to a highly nonlinear and non-convex problem and is solved by a local optimization method, thus only local optimality is guaranteed. They addressed some important constraints in their formulation but left out the friction circle constraint, which does not fully exploit the acceleration capacity of the vehicle.

By taking some additional steps beyond the seminal work done by [7], [8], we present a general speed planning framework specifically for autonomous driving that is able to handle a wide range of different scenarios using convex optimization subject to a large collection of relevant constraints. Our contributions are twofold. **(I)** We present a novel, general, flexible and complete mathematical model for speed planning, including friction circle, dynamics, smoothness, time efficiency, time window, and boundary condition constraints. We addressed the limitations of Lipp *et al*. [7] by introducing a *pseudo jerk* objective in longitudinal dimension to improve smoothness, adding time window constraints at certain point of the path to avoid dynamic obstacles, imposing a boundary condition at the end point of the path to guarantee safety for precise stop or merging scenarios. Compared to the approach of Liu *et al*. [6], our formulation optimizes the time efficiency directly while still staying inside of the friction circle, which ensures our method exploits the full acceleration capacity of the vehicle when necessary. **(II)** We demonstrate that our problem preserves convexity with the added constraints, and hence, that global optimality is guaranteed. This means our problem can be solved using state-of-the-art convex optimization solvers efficiently as well.

This paper is organized as follows. Section II formulates the problem for speed planning along a fixed path by considering different constraints. Section III demonstrates three case studies with parameters from real platforms. Section IV draws conclusions.

II. PROBLEM FORMULATION

Assuming a curvature continuous path is given, the speed planning problem seeks to find a time-efficient, safe, and smooth speed profile traveling along the fixed path which satisfies both safety and performance constraints.

In order to solve the proposed problem, we optimize over two performance criteria, smoothness, J_S, and time efficiency, J_T, with all other conditions encoded as hard constraints. We first introduce the path representation and explain the relationship of an arc-length parametrized path and a time parametrized path, then present mathematical expressions of all constraints, and finally, pose the complete optimization problem.

A. Path Representation

A workspace path, r, of the body point, b, at the center of the rear axle with footprint, $\mathcal{A}$, is defined as $r : [0, s_f] \rightarrow \mathbb{R}^2$. More specifically, we consider the following arc-length parametric form in a Cartesian coordinate system,

$$r(s) = (x(s), y(s)), s \in [0, s_f], \tag{1}$$

where s is the arc-length parameter along the path, $x(s)$ and $y(s)$ are the scalars along two orthogonal base axes respectively. The relationship between the arclength s and the corresponding time t is formed as the function $s = f(t)$, therefore the time parameterized workspace path $\tilde{r}(t) = (\tilde{x}(t), \tilde{y}(t)), t \in [0, t_f]$ can be easily acquired by substituting in for s.

Since the path, $r(s)$, is known, the speed vector $\vec{\boldsymbol{v}}$ in Cartesian coordinates can be calculated as below[1],

$$\vec{\boldsymbol{v}} = \dot{r}(s) = r'(s)\dot{f}, \tag{2}$$

where $r'(s)$ is the unit tangent vector of the path $r(s)$ at s that represents the direction of the speed of a car by assuming no sliding, $\dot{f}$ is the corresponding longitudinal speed of the car in ego frame. Let $\theta(s)$ represent the heading of the car at s of the path r, we get

$$r'(s) = \big(\cos(\theta(s)), \sin(\theta(s))\big) = \big(x'(s), y'(s)\big). \tag{3}$$

The acceleration vector $\vec{\boldsymbol{a}}$ in Cartesian coordinates system is

$$\vec{\boldsymbol{a}} = \ddot{r}(s) = r''(s)\dot{f}^2 + r'\ddot{f}, \tag{4}$$

where $\ddot{f}$ is the longitudinal acceleration and $r''(s)$ is the principle normal vector of the path, which is also called the curvature vector. The 2-norm of the $r''(s)$ is the scalar of the curvature

$$\kappa = \|r''\|. \tag{5}$$

[1]Throughout the paper, the prime $'$ and the dot $\cdot$ denote derivatives with respect to arc-length, s, and time, t, respectively.

B. Vehicle Model and Vehicle Dynamics Constraints

In order to describe the vehicle dynamics explicitly in the problem formulation, we employ the single track vehicle model [9] (see Fig. 1(b)) to represent the actual vehicle kinematics and dynamics, which is widely used in motion planning research [2], [3] and performs satisfactorily in practice [10]. The control force is defined as $\boldsymbol{u} = (u^\tau, u^\eta)$, where u^η is the lateral force and u^τ is the longitudinal force in the ego frame. The dynamics of the car are given by

$$R\boldsymbol{u} = m\ddot{r}, \tag{6}$$

where $R = \begin{bmatrix} \cos(\theta(s)) & -\sin(\theta(s)) \\ \sin(\theta(s)) & \cos(\theta(s)) \end{bmatrix}$ is the rotation matrix that maps forces from the ego frame to the global Cartesian coordinate system, m is the mass of the car. We replace the $\ddot{f}$ with a function $\alpha(s)$, $\dot{f}^2$ with a function $\beta(s)$ according to [8],

$$\alpha(s) = \ddot{f}, \beta(s) = \dot{f}^2. \tag{7}$$

Then, $\dot{\beta}(s) = 2\ddot{f}\dot{f} = 2\alpha(s)\dot{f} = \beta'\dot{f}$. Thus,

$$\beta'(s) = 2\alpha(s), s \in [0, s_f]. \tag{8}$$

Therefore, equation (4), (6), and (8) form the dynamics constraints of cars.

C. Friction Circle Constraints

The combination of lateral and longitudinal control forces that can be leveraged by cars should stay inside a friction circle to prevent slipping dramatically or operating outside the linear tire response region, which is defined as below

$$\|\boldsymbol{u}\| \leq \mu m g, \tag{9}$$

where μ is the coefficient of friction between the tires and the road surface. The longitudinal force upper boundary can be calculated according to the maximum longitudinal acceleration by $u^\tau \leq m \cdot a^\tau_{max}$. This is only a necessary condition but not a sufficient condition to limit decision variables within the physical limits such as the nominal power. Take a driving case along a straight line for example, the speed will constantly increases to infinity if a fixed longitudinal force acts on the car and the path is long enough. But in reality, the maximum force that a plant system can provide is also limited by the nominal power of the engine. For most operation, the actual power used by car systems is maintained below the nominal power P, shown as below,

$$u^\tau \dot{f} \leq P, \tag{10}$$

which also means that if the nominal power is reached, the driving force that a car is able to provide will decrease when the speed increases. This constraint is strictly nonlinear and non-convex, leading to challenges during optimization. This issue is ignored by [7], and was first pointed out by Zhu *et al.* in [11], but they did not solve it. Here, we provide our solution by adding an upper boundary constraint on speed profiles according to platform limits. It will prevent the speed from increasing without limits. By doing so, we partially address this issue without bringing in non-convexity to our problem formulation. Given these factors, the formal mathematical representation of the friction circle constraints can be defined as below,

$$\begin{aligned} \big(\alpha(s), \beta(s), \boldsymbol{u}(s)\big) \in \Big\{ \big(\ddot{r}(s), \dot{r}^2(s), \boldsymbol{u}(s)\big) \;\big|\; & \\ \|\boldsymbol{u}(\boldsymbol{s})\| \leq \mu m g, & \\ u^\tau(s) \leq m \cdot a^\tau_{max}, & \\ \beta(s) \leq v^2_{max} \Big\} & \end{aligned} \tag{11}$$

D. Time Efficiency Objective

Different from the approach used in [6] that optimizes deviation between the planned speed and desired speed to ensuring time efficiency implicitly, we optimize the total traveling time along the fixed path from 0 to s_f directly, similar to [7], [8], which can be expressed as $J_T = T = \int_0^T 1 dt$. By substituting the time variable t with arclength s, we arrive at the following expression for the time efficiency objective,

$$J_T = T = \int_{f(0)}^{f(t_f)} \frac{1}{\dot{f}} ds = \int_0^{s_f} \beta(s)^{-\frac{1}{2}} ds \tag{12}$$

E. Smoothness Objective

In order to ensure a smooth speed profile for better tracking performance, reduced wear of power train systems and improved ride comfort, the smoothness of the trajectory needs to be considered. Assuming that a smooth and curvature-continuous path is given, we only consider the longitudinal jerk component of the trajectory. According to (7) and (8), the jerk $\mathcal{J}(s)$ of the speed profile can be calculated as follows,

$$\begin{aligned} \mathcal{J}(s) = \dddot{f} = \dot{\alpha}(s) = \alpha'(s)\dot{f} & \\ = \alpha'(s)\sqrt{\beta(s)} = \frac{1}{2}\beta''(s)\sqrt{\beta(s)}, & \end{aligned} \tag{13}$$

which is nonlinear and non-convex. In fact, various smoothness metrics, including jerk, have been proposed in the literature to quantify the motion smoothness [12]. However, the jerk objective brings in non-linearity and non-convexity, which makes our problem hard to solve, a better measurement which covers all the aspects we care about and also with good mathematical properties should be selected for the sake of fast convergence rate and optimality. Therefore, we introduce a ***pseudo jerk***, $\alpha'(s)$, the first derivative of acceleration with respect to the arc-length, s, to the problem to encourage smooth transitions between states. The smoothness objective is then defined as

$$J_S = \int_0^{s_f} \|\alpha'(s)\|^2 ds, \tag{14}$$

which is convex.

F. Boundary Condition Constraints

The boundary condition constraints specifically refer to the terminal constraints that can be generally represented by

$$\begin{aligned} \underline{\alpha}_{s_f} \leq \alpha(s_f) \leq \bar{\alpha}_{s_f} \\ \underline{\beta}_{s_f} \leq \beta(s_f) \leq \bar{\beta}_{s_f}. \end{aligned} \tag{15}$$

where $\underline{\alpha}_{s_f}$, $\underline{\beta}_{s_f}$ are the lower boundaries and $\bar{\alpha}_{s_f}$, $\bar{\beta}_{s_f}$ are the upper boundaries. These constraints involve two types of typical applications. One is the scenario that the car needs to fully stop in front of an obstacle at a certain point on the path or at the end of the path. A zero speed and a zero acceleration at s_f need to be guaranteed in this case. The other scenario occurs as a car tries to merge into an expressway from an entrance ramp, which needs to have the final speed fall in the speed limit range of the expressway. Other applications, such as keeping a fixed distance to the front car at the end of the path while matching the final speed with that of the front car, can also be easily solved using this constraint in our framework. Such capabilities are not present in [6], [7]. If no strict boundary conditions on terminal states are required, the constraints can be deactivated by making $\underline{\alpha}_{s_f} = -\mu g$, $\underline{\beta}_{s_f} = 0$, $\bar{\alpha}_{s_f} = \mu g$, $\bar{\beta}_{s_f} = v_{max}^2$.

G. Time Window Constraints

Time window constraints are represented as

$$t_i = T(s_i) \in W_T = (0, T_U] \tag{16}$$

where $T(s_i) = \int_0^{s_i} \beta(s)^{-\frac{1}{2}} ds$ and $T_U > 0$. The constraint ensures that if the car passes the station s_i during the time window W_T, non-collision with other traffic participants is guaranteed. The time window, W_T, can be acquired efficiently from a collision detection algorithm such as [13] with predicted trajectories of traffic participants in the workspace-time space. This type of constraint is very useful for handling time-critical tasks such as dynamic obstacle avoidance at certain points, s_i, along the path, and for arriving at the destination within the given maximum time duration. If no time window information about dynamic obstacles is available, this constraint can be relaxed by setting $T_U = \infty$.

H. Overall Convex Optimization Problem Formulation

Finally, the complete speed planning optimization problem over the fixed path is posed, which incorporates the full set of constraints presented above as,

$$\begin{aligned} \underset{\alpha(s),\beta(s),u(s)}{\textbf{minimize}} \quad & J = J_T + \omega J_S \\ \text{s.t.} \quad & (6), (8), (11), (15), (16), \end{aligned} \tag{17}$$

where $\dot{r}^2(s) = \big(r'(s)\big)^2 \beta(s)$ and $\ddot{r}(s) = r'\alpha(s) + r''\beta(s)$. Note that $\alpha(s)$, $\beta(s)$, $u(s)$ are the decision variables to optimize. The parameter $\omega \in \mathbb{R}_+$ is fixed in advance to suit the particular application objectives. The problem formulation we presented can be demonstrated to be convex as follows. **(I)** For the objectives, J_T is an integral of a negative power function and is therefore convex. J_S is an integral of a squared power of absolute value and is therefore convex. As ω is nonnegative, J, as a nonnegative weighted sum of convex functions, is convex. **(II)** For (6), the dynamics equality constraint is affine in α, β, u and is therefore convex. For the equality constraints about decision variables (8), since the derivative is a linear operator, the relation between α and β is convex. For the convex set constraint about the friction circle (11), the norm of u is convex, upper bounds are fixed and v_{max}^2 is fixed, so the control set constraint is the intersection of three convex sets and is therefore convex. The equality and inequality constraints about boundary conditions (15) are linear constraints, thus convex. As the t_i is an integral of a negative power function, therefore convex and T_U is a fixed upper boundary, the time window inequality constraint (16) is a convex constraint.

Since the objectives are convex, equality contraints are affine and inequality constraints are convex, this optimization problem is convex [14]. The speed planning problem as stated is therefore an infinite-dimensional convex optimization problem. We model our problem using Convex.jl [15] , a convex optimization modeling framework in Julia, and solve it using a second-order cone programming solver from Gurobi [16].

III. CASE STUDY

In this section, we demonstrate the effectiveness of the proposed methods by comparing our results with MTSOS [7], and show both improvements and the new capabilities in multiple case studies for both static and dynamic environments.

TABLE II: Parameter Values

Parameter	Description	Values	Unit
w	Car width	2.45	m
l	Car length	4.9	m
wb	Car wheelbase	2.8448	m
tr	Car track	1.5748	m
m	Mass of the car.	1500.0	kg
μ	Friction coefficient	0.7	1
g	Acceleration due to gravity	9.83	m/s^2
a_c^η	Longitudinal acceleration threshold for comfort	$0.4 \cdot \mu g$	m/s^2
a_c^τ	Lateral acceleration threshold for comfort	$0.4 \cdot \mu g$	m/s^2
a_{max}^τ	Max. longitudinal acceleration of the car	$0.5 \cdot \mu g$	m/s^2
v_{max}	Max. speed of the car	30	m/s

A. Safe Stop with A High Entry Speed

We considered a cornering scenario (see Fig. 2(a)) with a high entry speed of $12m/s$. At the end of the path, a static obstacle blocks the road, and th car must stop safely in front of the obstacle. First, we perform speed planning using the problem formulation from [7], which only considers the time efficiency objective, dynamics, and friction circle constraints. As there is no terminal constraint included, the final speed is free and the vehicle does not stop for the obstacle. The resulting speed profile is shown as a black curve in Fig. 3. By adding the terminal boundary condition constraint, our method is able to conduct a safe stop precisely (see curves ***A*-*D*** in Fig. 3). Further, the results from MTSOS with only the time efficiency considered include multiple cusps, which significantly increase the difficulty of tracking the proposed

reference speeds. Due to the time efficiency objective, most of the control efforts tend to stay on the limits of the friction circle, shown as the black dots in Fig. 2(b). Overshoot and oscillation may occur when tracking a non-smooth speed profile such as the MTSOS curve or curve ***A*** in Fig. 3. By adding the proposed smoothness objective with different weights $\omega = 0.001$, $\omega = 0.01$, $\omega = 0.1$, our method can generate variable smoothness speed profiles, depicted as curves ***B***, ***C***, and ***D*** in Fig. 3, respectively. As the coefficient of smoothness increases, higher speed profiles slopes are penalized more heavily, thus smoother speed profiles are generated. The acceleration points of curve ***B*** and curve ***D*** were also drawn in Fig. 2(b) as green dots and light blue dots respectively. As the smoothness coefficients increase, the acceleration points distribution tend to lie closer to the center of the friction circle and reach the limits less frequently, which leads to a gentler control sequence.

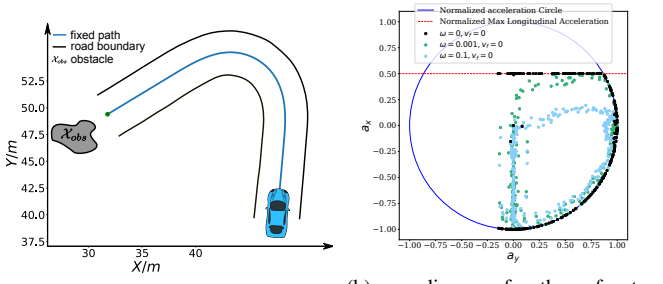

(a) Safe stop scenario

(b) g-g diagram for the safe stop scenario

Fig. 2

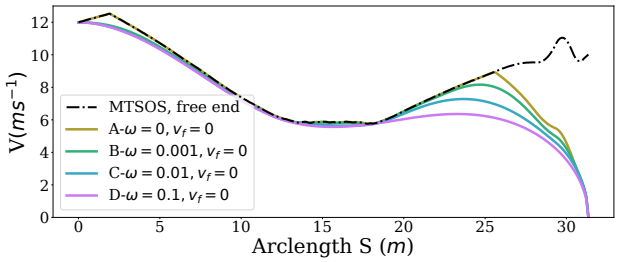

Fig. 3: Speed profiles for the safe stop scenario

B. Dealing with Jaywalking on A Curvy Road

Second, we consider a jaywalking scenario on a curvy road. The time window $[t_1 = 7s, t_2 = 11s]$ that the pedestrian occupies the road at $s = 30m$ is given by a dynamic obstacle prediction subsystem. As shown in the previous experiments, our method is able to stop at a specified point along the path. Here, we consider two advanced use cases to avoid the pedestrian safely without stopping by manipulating the arrival time. Non-stop dynamic obstacle avoidance strategies may result in energy saving driving behavior or greatly reduced operation time in certain cases. As the pedestrian occupies the road between 7s and 11s at $s = 30m$ along the path, if our car reaches $s = 30m$ in the same time window, an accident may happen. Unfortunately, with the parameter setting $\omega = 5$, our car will collide with the pedestrian, which is shown as the green curve in Fig. 5. Two strategies can be employed to avoid this failure. The first involves passing the potential collision point before the pedestrian arrives point A, that is, $t_{s=30m} <= t_1$, which is shown as the blue car situation in Fig. 4. The second involves passing the potential collision point just after the pedestrian passes point B, that is, $t_{s=30m} >= t_2$, which is shown as a green car situation in Fig. 4. We solve this problem using both strategies. By making $\omega = 15, t_{s=30m} <= 6.8s$, we solve the former case and the corresponding results are demonstrated in cyan in Fig. 5 and Fig. 6. In practice, we may be not able to pass the barrier in time using the former strategy due to dynamics constraints of cars. The latter approach or a safe stop at a specified point along the path can be always employed to avoid collision. The latter approach is solved by setting $\omega = 15, t_{s=30m} <= 11.2s$. The results are presented in pink in Fig. 5 and Fig. 6. It should be noted that the second approach is an indirect method for avoiding collision in this scenario. We first stretch the time by increasing the coefficient ω from 5 to 15, then compress the arrival time by making $t_{s=30m} \leq 11.2s$. The exact arrival time at $s = 30m$ for three different cases are $10.026s$ (green), $6.799s$ (cyan), and $11.199s$ (pink).

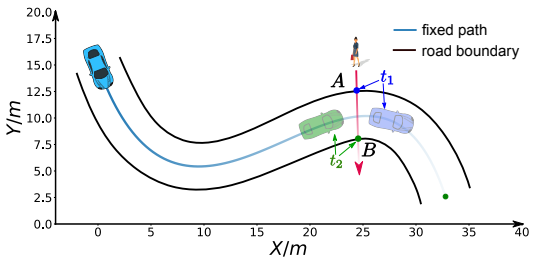

Fig. 4: Jaywalking scenario

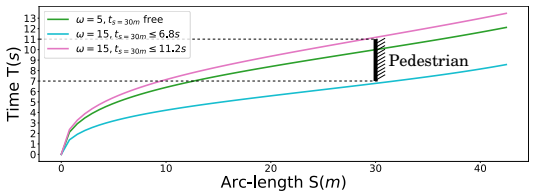

Fig. 5: S-T graph for the jaywalking scenario

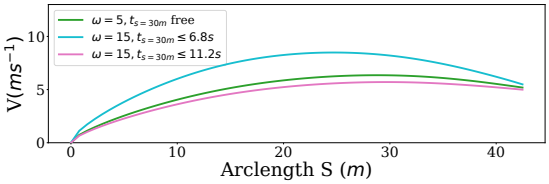

Fig. 6: S-V graph for the jaywalking scenario

C. Speed Planning for Freeway Entrance Ramp Merging

Finally, we demonstrate a freeway entrance ramp merging scenario. The oncoming yellow car is driving in around $20m/s$. The arrival time $t_A = 8.5s$ at merging point A in Fig. 7 is given by the dynamic obstacle prediction or a V2V communication module. The initial speed of the autonomous driving car is $4m/s$. With the parameter setting $\omega = 8$, $20m/s \leq v_f \leq 22m/s$, the arrival time t_{s_f} at position B of the autonomous car provided by the optimization is $10.557s$. The related speed profile is shown as the green curve in Fig. 8. The corresponding S-T graph is depicted in Fig. 9 in green. The trajectory of the oncoming car is shown as the black curve in Fig. 9. The scenario is designed such that the autonomous car would collide with the oncoming vehicle in the conflict zone if the oncoming car does not yield. To avoid the risk, we enforce a time window constraint at the end of the path, based on the previous parameter settings, by making $t_f \leq 8.5s$. In this way, the autonomous vehicle has already reached position B by the time the oncoming vehicle arrives at position A, which also keeps a safe distance between the two vehicles. Further, the final speed of the autonomous car is constrained to be no less than that of the oncoming vehicle, which ensures that safety is guaranteed. The corresponding solution is depicted by the cyan curve in Fig. 8 and Fig. 9. The exact arrival time of the autonomous car at the end the path is $8.5s$.

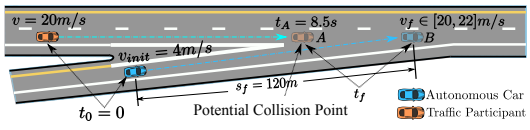

Fig. 7: Freeway entrance ramp merging scenario

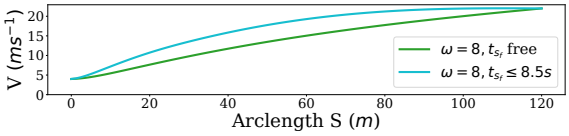

Fig. 8: S-V graph for the freeway entrance ramp merging scenario

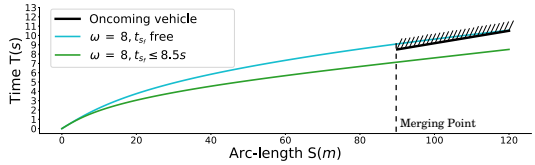

Fig. 9: S-T graph for the freeway entrance ramp merging scenario

IV. CONCLUSIONS

In this paper, we present a general, complete and flexible speed planning approach which includes time efficiency, friction circle, vehicle dynamics, smoothness, time window, and boundary conditions for speed planning along a fixed path. The method is able to handle a wide range of speed planning problems raised in different scenarios in both static and dynamic environments while providing high-quality, time-efficient, safety-guaranteed, dynamically-feasible solutions in a unified framework. We also demonstrate that our problem formulation remains the convexity with all the constraints added, which means the global optimality are guaranteed. We showcase how our method can be used to solve speed planning problems by providing several typical case studies in both static and dynamic environments. These results have shown that the proposed method outperforms existing speed planners for autonomous driving in terms of constraint type covered, optimality, safety, mobility.

REFERENCES

[1] J. Ziegler, P. Bender, T. Dang, and C. Stiller, "Trajectory planning for bertha – a local, continuous method," in *IEEE Intelligent Vehicles Symposium (IV)*, 2014, pp. 450–457.

[2] M. McNaughton, C. Urmson, J. M. Dolan, and J.-W. Lee, "Motion planning for autonomous driving with a conformal spatiotemporal lattice," in *IEEE International Conference on Robotics and Automation (ICRA)*, 2011, pp. 4889–4895.

[3] T. Gu, "Improved trajectory planning for on-road self-driving vehicles via combined graph search, optimization & topology analysis," Ph.D. dissertation, Carnegie Mellon University, 2017.

[4] X. Li, Z. Sun, D. Cao, Z. He, and Q. Zhu, "Real-time trajectory planning for autonomous urban driving: Framework, algorithms, and verifications," *IEEE/ASME Transactions on Mechatronics*, vol. 21, no. 2, pp. 740–753, apr 2016.

[5] A. Dakibay and S. L. Waslander, "Aggressive vehicle control using polynomial spiral curves," in *IEEE 20th International Conference on Intelligent Transportation Systems (ITSC)*, 2017, pp. 1–7.

[6] C. Liu, W. Zhan, and M. Tomizuka, "Speed profile planning in dynamic environments via temporal optimization," in *IEEE Intelligent Vehicles Symposium (IV)*, 2017, pp. 154–159.

[7] T. Lipp and S. Boyd, "Minimum-time speed optimisation over a fixed path," *International Journal of Control*, vol. 87, no. 6, pp. 1297–1311, feb 2014.

[8] D. Verscheure, B. Demeulenaere, J. Swevers, J. De Schutter, and M. Diehl, "Time-optimal path tracking for robots: A convex optimization approach," *IEEE Transactions on Automatic Control*, vol. 54, no. 10, pp. 2318–2327, oct 2009.

[9] R. Rajamani, *Vehicle Dynamics and Control*. Springer US, 2012.

[10] P. Polack, F. Altché, B. d'Andréa Novel, and A. de La Fortelle, "The kinematic bicycle model: A consistent model for planning feasible trajectories for autonomous vehicles?" in *IEEE Intelligent Vehicles Symposium (IV)*, 2017, pp. 812–818.

[11] Z. Zhu, E. Schmerling, and M. Pavone, "A convex optimization approach to smooth trajectories for motion planning with car-like robots," in *IEEE 54th Annual Conference on Decision and Control (CDC)*, 2015, pp. 835–842.

[12] S. Balasubramanian, A. Melendezcalderon, A. Robybrami, and E. Burdet, "On the analysis of movement smoothness," *Journal of Neuro-Engineering and Rehabilitation*, vol. 12, no. 1, p. 112, dec 2015.

[13] U. Schwesinger, R. Siegwart, and P. Furgale, "Fast collision detection through bounding volume hierarchies in workspace-time space for sampling-based motion planners," in *2015 IEEE International Conference on Robotics and Automation (ICRA)*, may 2015, pp. 63–68.

[14] S. Boyd and L. Vandenberghe, *Convex Optimization*. Cambridge University Press, 2004.

[15] M. Udell, K. Mohan, D. Zeng, J. Hong, S. Diamond, and S. Boyd, "Convex optimization in julia," in *Proceedings of the 1st First Workshop for High Performance Technical Computing in Dynamic Languages*, ser. HPTCDL '14. Piscataway, NJ, USA: IEEE Press, 2014, pp. 18–28.

[16] G. Optimization, "Gurobi optimizer reference manual; gurobi optimization," *Inc.: Houston, TX, USA*, 2016.